

Water-wave turbulence: statistics beyond the spectra.

Yuri V. Lvov¹, Sergey Nazarenko², Boris Pokorni¹

¹ Department of Mathematical Sciences, Rensselaer Polytechnic Institute, Troy NY 12180

² The University of Warwick, Coventry CV4 7AL, UK

February 25, 2019

Abstract

We perform numerical simulations of the dynamical equations for free water surface in presence of gravity in order to compare the numerically obtained statistics with the assumptions and predictions of the Wave Turbulence (WT) theory. Such a theory was derived under a weak nonlinearity assumption and in the infinite basin limit. Thus, its robustness is not obvious for larger nonlinearity levels which are necessary in numerics to activate the cascade in the discrete k -space and to reduce the computational time to an affordable level. As in several other recent numerical studies [1–3], we confirm the Zakharov-Filonenko spectrum predicted by WT. We also go beyond finding the spectra and compute the one-mode probability density function (PDF) of the wave amplitudes. In agreement with recently developed theory [4, 5], this PDF is found to show an anomalously large, with respect to Gaussian fields, probability of strong waves. Also in agreement with the theory, we find that phases ϕ_k are correlated whereas factors $e^{i\phi_k}$ are de-correlated. However, at odds with the traditional WT picture, we find that at each k there are two types of oscillations present: a dominant component at the linear frequency and a weaker one with a nonlinear frequency shift. We further observe that the energy cascade is very “bursty” in time and is somewhat similar to sporadic sandpile avalanches. We explain this as a cycle: a cascade arrest due to discrete k ’s leads to accumulation of energy near the forcing scale which, in turn, leads to widening of the nonlinear resonance and, therefore, triggering of the cascade draining the turbulence levels and returning the system to the beginning of the cycle.

1 Introduction

Water waves have fascinated humans since ancient times. If you ask a child to draw waves, there is no doubt you will get a picture of waves on sea, perhaps with a little boat floating on them. Such a drawing would also give you a pretty accurate assessment of why it is important to understand and predict waves: for good navigation. Surface gravity waves are also important for the momentum

transfer from wind to sea, absorption of oxygen and CO_2 by water, spreading of surface pollutants and zooplankton, predicting and avoiding hazards of underwater oil drilling.

Normal state of the sea surface is chaotic with a lot of waves at different scales propagating in random directions. Such a state is referred to as Wave Turbulence (WT). Theory of WT was developed by finding a statistical closure based on the small nonlinearity and on the Wick splitting of the Fourier moments, the later procedure is often interpreted as closeness of statistics to Gaussian or/and to phase randomness (the two are not the same, see [4–6]). This closure yields a wave-kinetic equation (WKE) for the waveaction spectrum. Such WKE for the surface waves was first derived by Hasselmann [7]. A significant achievement in WT theory was to realize that the most relevant states in WT are energy cascades through scales similar to the Kolmogorov cascades in Navier-Stokes turbulence, rather than thermodynamic equilibria as in the statistical theory of gases. This understanding came when Zakharov and Filonenko found an exact power-law solution to WKE which is similar to the famous Kolmogorov spectrum [8]. In terms of frequency ω , the Zakharov-Filonenko (ZF) spectrum scales as ω^{-4} and this scaling was experimentally observed by Toba [9]. Confirmation of ZF spectra and computing other (e.g. unsteady) spectra have so far dominated in the numerical studies of WT. By now, one can say with confidence that ZF spectrum is indeed observed even in the situations which are formally beyond the validity limits of its theoretical derivation, e.g. when nonlinearity becomes not-so-small or when the wave forcing is anisotropic [2]. On the other hand, it has also been realized that WT cannot be completely Gaussian and, in particular, Gaussianity may be “spoiled” by coherent events such as wavebreaking (at small scales) [10, 11] or freak waves (large scales) [12]. Clearly, non-Gaussianity and the degree to which the wave modes are random or coherent cannot be judged based on the spectra and one has to study higher-order statistics. Recently, such an attempt was made in a numerical study of the surface gravity waves by Yokoyama [3] who computed the structure functions in the coordinate space for the surface elevation and its Laplacian. Such non-Gaussianity was found for the long-wave part of the spectrum, and it was attributed to generation of Stokes-like nonlinear wave structures which are possibly related to the freak waves.

In Navier-Stokes turbulence, one normally studies the real-space structure functions. On the other hand, the Fourier space is more fundamental for weakly nonlinear waves because in the linear limit “turbulence” is just a superposition of independent Fourier modes oscillating at their own frequency fully determined by the wavenumber. Thus, WT predictions have been made for the k -space quantities. Traditionally WT has been used to predict the energy spectrum and, as a result, most of numerical studies aimed at testing WT were concerned solely with the spectrum. However, recently WT was extended to study other important statistical quantities and predictions were made about the higher moments of the wave amplitudes, their PDF’s and the statistical behaviour of the phase. Thus, our primary goal in the present paper will be to simulate the free surface equations in order to measure the k -space statistics (beyond the spectrum) and to compare it with the WT predictions. Besides the fact that the predictions of WT are made for the Fourier space objects, the statistical properties which are fundamental for the WT closure itself are also formulated in the Fourier space. Specifically, the amplitudes and the phases of all of the Fourier modes have to make a set of independent random variables [4–6] and this property can and should be examined numerically.

Numerical simulation of the moving water surface is a challenging problem due to a tremendous amount of computing power required for computing weakly nonlinear dispersive waves. This arises due to presence of widely separated spatial and time scales. As will be explained below, the weaker we take nonlinearity, the larger we should take the computational box in order to overcome the k -space discreteness and ignite wave resonances leading to the energy cascade through scales. In order to maximise the inertial range, one tries to force at the lowest wavenumbers possible, but without forgetting that the forcing should be strong enough for the resonance broadening to overcome the discreteness effect. In this paper we estimate the minimal resonance broadening which is sufficient to generate the cascade. In our numerics, we will maintain turbulence levels with an order of magnitude greater broadening than this minimal value in order to lower the anisotropy effects. Although these turbulence levels are such that the broadening is still less than the k -grid spacing at low k , we find that the nonlinear effects are large in most of the k -space. This is due to the fact that nonlinearity tends to grow along the energy cascade toward high k 's [10, 11] and, therefore, we cannot minimise both the discreteness and the nonlinearity effects given the numerical resolution affordable to us today.

Thus, it is necessary to examine whether the WT predictions hold in the numerical simulations in which the discreteness and nonlinearity are still significant and the formal applicability conditions of WT are violated. As in other recent numerical experiments [1–3], here we confirm formation of the ZF spectrum corresponding to the direct energy cascade. Further, in agreement with more recent WT predictions about the higher-order statistics [4, 5], we observe an anomalously high (with respect to Gaussian) probability of the large-amplitude waves. Also in agreement with recent WT findings [5], we observe a buildup of strong correlations of the wave phases ϕ_k whereas the factors $e^{i\phi_k}$ remain de-correlated.

However, we find a fundamental disagreement with the traditional WT view that the lowest order nonlinearity effect on the modes is to shift the linear frequency by ω_{NL} . Instead, by analysing the phase behaviour and the time-Fourier transform we find that two components are present at each k : a dominant one oscillating at (very close to) linear frequency ω_k , and a weaker component with a frequency shift whose value is less and is of the opposite sign with respect to ω_{NL} . In absence of nonlinearity one would observe only the first but not the second peak and, therefore, one can quantify the nonlinearity level as the ratio of the amplitudes of these two peaks. When the second peak becomes stronger than the first one, the wave phase experiences a rapid and persistent monotonic change. Detecting such phase “runs” gives an interesting picture of the nonlinear activity in the 2D k -space. In particular, we notice a “bursty” nature of the energy cascade resembling sandpile avalanches. Possible explanation of such behaviour is the following. When nonlinearity is weak, there is no wave-wave resonances, consequently there is no effective energy transfer, and system behaves like “frozen turbulence” (term introduced in [13] for the capillary wave turbulence). Energy generated at the forcing scale will accumulate near this scale and the nonlinearity will grow. When resonance broadening gets wide enough, so that the resonances are not inhibited by discreteness, the nonlinear wave-wave energy transfer starts, which diminishes nonlinearity and subsequently “arrests” resonances. Thus the system oscillates between having almost linear oscillations with stagnated energy and occasional avalanche-like discharges.

2 Equations for the free surface

Let us consider motion of a water volume of infinite depth embedded in gravity and bounded by a surface separating it from air at height $z = \eta(\mathbf{x}, t)$ where $\mathbf{x} = (x, y)$ is the horizontal coordinate. Let the velocity field be irrotational, $\mathbf{u} = \nabla\Phi$, so that the incompressibility condition becomes

$$\Delta\Phi = 0, \quad \text{for } z < \eta(\mathbf{x}, t). \quad (1)$$

Rate of change of the surface elevation must be equal to the vertical velocity of the fluid particle on this surface, which gives

$$D_t\eta = \partial_z\Phi, \quad \text{for } z = \eta(\mathbf{x}, t), \quad (2)$$

where $D_t = \partial_t + \mathbf{u} \cdot \nabla_\perp$ is the material time derivative. The second condition at the surface arises from the Bernoulli equation in which pressure is taken equal to its atmospheric value. This condition gives

$$\partial_t\Phi + \frac{1}{2}|\nabla\Phi|^2 = -g\eta, \quad \text{for } z = \eta(\mathbf{x}, t), \quad (3)$$

where g is the free-fall acceleration.

Although equations (2) and (3) involve only two-dimensional coordinate \mathbf{x} , the system remains three-dimensional due to the 3D equation (1). One can transform these equations to a truly 2D form by assuming that the surface deviates from its rest plane only by small angles and by truncating the nonlinearity at the cubic order with respect to the small deviations. This procedure yields the following dynamical equations (see e.g. [14]):

$$\begin{aligned} \eta_t &= \mathbf{\Gamma}[\Psi] \\ &\quad -\varepsilon(\mathbf{\Gamma}[\mathbf{\Gamma}[\Psi]\eta] + \nabla_\perp \cdot [(\nabla_\perp\Psi)\eta]) \\ &\quad +\varepsilon^2\left(\mathbf{\Gamma}[\mathbf{\Gamma}[\mathbf{\Gamma}[\Psi]\eta]\eta] + \frac{1}{2}\mathbf{\Gamma}[(\Delta_\perp\Psi)\eta^2] + \frac{1}{2}\Delta_\perp(\mathbf{\Gamma}[\Psi]\eta^2)\right), \end{aligned} \quad (4)$$

$$\begin{aligned} \Psi_t &= -g\eta \\ &\quad -\varepsilon\frac{1}{2}(|\nabla_\perp\Psi|^2 - (\mathbf{\Gamma}[\Psi])^2) \\ &\quad -\varepsilon^2\mathbf{\Gamma}[\Psi](\mathbf{\Gamma}[\mathbf{\Gamma}[\Psi]\eta] + (\Delta_\perp\Psi)\eta), \end{aligned} \quad (5)$$

where

$$\Psi = \Phi|_{z=\eta(\mathbf{x}, t)}, \quad (6)$$

and $\mathbf{\Gamma}$ is the Gilbert transform which in the Fourier space corresponds to multiplication by $k = |\mathbf{k}|$, i.e.

$$\mathbf{\Gamma}[f](\mathbf{x}, t) = \frac{1}{2\pi} \int k \widehat{f}(\mathbf{k}, t) e^{i\mathbf{k}\cdot\mathbf{x}} d\mathbf{k}.$$

Here, we have the following convention for defining the Fourier transform

$$\widehat{f}(\mathbf{k}) = \frac{1}{2\pi} \int e^{i(\mathbf{k}\cdot\mathbf{x})} f(\mathbf{x}) d\mathbf{x}. \quad (7)$$

In equations (4) and (5), we rescaled variables η and Ψ to make them order one, so that the nonlinearity smallness is now in a formal parameter $\epsilon \ll 1$.

Truncated equations (4) and (5) will be used for our numerical simulations. They have a convenient form for the pseudo-spectral method which computes evolution of the Fourier modes but switches back to the coordinate space for computing the nonlinear terms. However, for theoretical analysis these equations have to be diagonalised in the k -space and a near-identity canonical transformation must be applied to remove the nonlinear terms of order ϵ since the gravity wave dispersion $\omega = \sqrt{gk}$ does not allow three-wave resonances. The resulting equation is also truncated at ϵ^2 order and it is called the Zakharov equation [15–18],

$$i\dot{a}_l = \epsilon^2 \sum_{\alpha\mu\nu} W_{\mu\nu}^{l\alpha} \bar{a}_\alpha a_\mu a_\nu e^{i\omega_{\mu\nu}^{l\alpha} t} \delta_{\mu\nu}^{l\alpha}, \quad (8)$$

where $\omega_{\mu\nu}^{l\alpha} = \omega_l + \omega_\alpha - \omega_\mu - \omega_\nu$, $\omega_l = \sqrt{gk_l}$ is the frequency of mode \mathbf{l} ($\mathbf{l} \in \mathcal{Z}^2$), $\mathbf{k}_l = 2\pi\mathbf{l}/L$ is the wavenumber, L is the box size and $k_l = |\mathbf{k}_l|$. Here, a_l is the wave action variable in the interaction representation, $a_l = e^{i\omega_l t} b_l$ where b_l is a normal variable,

$$b_l = \sqrt{\frac{\omega_l}{2k_l}} \eta_l + i\sqrt{\frac{k_l}{2\omega_l}} \Psi_l + 0(\epsilon). \quad (9)$$

Here, $0(\epsilon)$ terms appear because of the near-identity canonical transformation needed to remove the quadratic terms from the evolution equations [15–20]. The correct expression for the interaction coefficient $W_{\mu\nu}^{l\alpha}$ was first derived in [20]. It is given by a long expression which will be given in Appendix (see (28)).

Note that although Zakharov equation is most suitable for theory, it is not convenient for computations because the possibility of computing the nonlinear term in the real space (as a simple product) is lost due to a complicated dependence of the interaction coefficient on the wavenumber.

3 Statistical Quantities in Wave Turbulence

Let us consider a wavefield in a periodic square basin of side L and let the Fourier representation of this field be $a_l(t)$ where index $\mathbf{l} \in \mathcal{Z}^2$ marks the mode with wavenumber $\mathbf{k}_l = 2\pi\mathbf{l}/L$ on the grid in the 2-dimensional Fourier space. Discrete k -space is important for formulating the statistical problem. For simplicity let us assume that there is a cut-off wavenumber k_{max} so that there is no modes with wavenumber components greater than k_{max} , which is always the case in numerical simulation. In this case, the total number of modes is $N = (k_{max}/\pi L)^2$ and index \mathbf{l} will only take values in a finite box, $\mathbf{l} \in \mathcal{B}_N \subset \mathcal{Z}^2$ which is centred at 0 and all sides of which are equal to $N^{1/2}$. To consider homogeneous turbulence, the large box (i.e. continuous k) limit, $N \rightarrow \infty$, will have to be taken later.

Let us write the complex a_l as $a_l = A_l \psi_l$ where A_l is a real positive amplitude and ψ_l is a phase factor which takes values on \mathcal{S}^1 , a unit circle centred at zero in the complex plane. The most general statistical object in WT [5] is the N -mode joint PDF $\mathcal{P}^{(N)}$ defined as the probability for the wave intensities A_l^2

to be in the range $(s_l, s_l + ds_l)$ and for the phase factors ψ_l to be on the unit-circle segment between ξ_l and $\xi_l + d\xi_l$ for all $\mathbf{l} \in \mathcal{B}_N$.

The fundamental statistical property of the wavefield in WT is that all the amplitudes A_l and phase factors ψ_l are independent statistical variables and that all ψ_l 's are uniformly distributed on \mathcal{S}^1 . This kind of statistics was introduced in [4–6] and called ‘‘Random Phase and Amplitude’’ (RPA) field. In terms of the PDF, we say that the field a is of RPA type if it can be product-factorised,

$$\mathcal{P}^{(N)}\{s, \xi\} = \frac{1}{(2\pi)^N} \prod_{\mathbf{l} \in \mathcal{B}_N} P_l^{(a)}(s_l), \quad (10)$$

where $P_l^{(a)}(s_l)$ is the one-mode PDF for variable A_l^2 .

Note that in this formulation the distributions of A_l remain unspecified and, therefore, the amplitudes do not have to be deterministic (as in earlier works using RPA) nor do they have to correspond to Gaussianity,

$$P_l^{(a)}(s_l) = \frac{1}{n_l} \exp(-s_l/n_l) \quad (11)$$

where $n_l = \langle s_l \rangle$ is the waveaction spectrum.

Importantly, RPA formulation involves independent *phase factors* $\psi = e^{i\phi}$ and not *phases* ϕ . Firstly, the phases would not be convenient because the mean value of the phases is evolving with the rate equal to the nonlinear frequency correction [5]. Thus one could not say that they are ‘‘distributed uniformly from $-\pi$ to π ’’. Moreover the mean fluctuation of the phase distribution is also growing and they quickly spread beyond their initial 2π -wide interval [5]. But perhaps even more important, it was shown in [5] that ϕ 's build mutual correlations on the nonlinear timescale whereas ψ 's remain independent. In the present paper we are going to check this theoretical prediction numerically by directly measuring the properties of ϕ 's and ψ 's.

In [4, 6] RPA was *assumed* to hold over the nonlinear time. In [5] this assumption was examined *a posteriori*, i.e. based on the evolution equation for the multi-point PDF. Note that only the phase randomness is necessary for deriving this equation, whereas both the phase and the amplitude randomness are required for the WT closure for the one-point PDF or the kinetic equation for the spectrum. This fact allows to prove that, if valid initially, the RPA properties survive in the leading order in small nonlinearity and in the large-box limit [5]. Such an approximate leading-order RPA is sufficient for the WT closure.

4 Theoretical WT predictions

When the wave amplitudes are small, the nonlinearity is weak and the wave periods, determined by the linear dynamics, are much smaller than the characteristic time at which different wave modes exchange energy. In the other words, weak nonlinearity results in a timescale separation and this fact is exploited in WT to describe the slowly changing wave statistics by averaging over the fast linear oscillations.

4.1 Evolution equations for the PDF's, moments and spectrum.

In [5] the following equation for the N -mode PDF was obtained for the four-wave systems,

$$\dot{\mathcal{P}} = \pi\epsilon^2 \int |W_{nm}^{jl}|^2 \delta(\tilde{\omega}_{nm}^{jl}) \delta_{nm}^{jl} \left[\frac{\delta}{\delta s} \right]_4 \left(s_j s_l s_m s_n \left[\frac{\delta}{\delta s} \right]_4 \mathcal{P} \right) d\mathbf{k}_j d\mathbf{k}_l d\mathbf{k}_m d\mathbf{k}_n, \quad (12)$$

where

$$\left[\frac{\delta}{\delta s} \right]_4 = \frac{\delta}{\delta s_j} + \frac{\delta}{\delta s_l} - \frac{\delta}{\delta s_m} - \frac{\delta}{\delta s_n}. \quad (13)$$

Here $N \rightarrow \infty$ limit has already been taken and $\frac{\delta}{\delta s_j}$ means the variational derivative. Using this equation, one can prove that RPA property holds over the nonlinear time, i.e. the N -mode PDF remains of the product factorised form with accuracy sufficient for the WT closures to work [5]. Using RPA, we get for the one-point marginals [5],

$$\frac{\partial P_a}{\partial t} + \frac{\partial F}{\partial s_j} = 0, \quad (14)$$

with F is a probability flux in the s -space,

$$F = -s_j \left(\gamma P_a + \eta_j \frac{\delta P_a}{\delta s_j} \right), \quad (15)$$

where

$$\eta_j = 4\pi\epsilon^2 \int |W_{nm}^{jl}|^2 \delta_{nm}^{jl} \delta(\omega_{nm}^{jl}) n_l n_m n_n d\mathbf{k}_l d\mathbf{k}_m d\mathbf{k}_n, \quad (16)$$

$$\gamma_j = 4\pi\epsilon^2 \int |W_{nm}^{jl}|^2 \delta_{nm}^{jl} \delta(\omega_{nm}^{jl}) \left[n_l (n_m + n_n) - n_m n_n \right] d\mathbf{k}_l d\mathbf{k}_m d\mathbf{k}_n. \quad (17)$$

Here we introduced the wave-action spectrum,

$$n_j = \langle A_j^2 \rangle. \quad (18)$$

From (14) we get the following equation for the moments $M_j^{(p)} = \langle A_j^{2p} \rangle$:

$$\dot{M}_j^{(p)} = -p\gamma_j M_j^{(p)} + p^2 \eta_j M_j^{(p-1)}. \quad (19)$$

which, for $p = 1$ gives the standard wave kinetic equation (WKE),

$$\dot{n}_j = -\gamma_j n_j + \eta_j. \quad (20)$$

4.2 Preservation of the RPA property.

Validity of the WT theory relies on persistence of the RPA property of the wavefield over the nonlinear evolution time. Such persistence was demonstrated in [5] based on the evolution equation for the multi-mode PDF, where the product factorisation of PDF was shown to hold with an accuracy sufficient for the WT closure. It was also emphasised in [5] that RPA must use independent phase factors ψ_k rather than the phases ϕ_k independence of which does not survive over the nonlinear time. The theoretical prediction of persistent independence of A_k 's and ψ_k 's and about the growth of correlations of ϕ_k 's will be checked in this paper numerically.

Further, the WT approach predicts that the mean value of the phase grows with a rate given by the nonlinear frequency correction and that the r.m.s. fluctuation of the phase also grows in time [5]. In this paper we will see that in reality the time evolution of the phase is more complicated than this WT prediction: the phase exhibits quasi-periodic fluctuations intermittent by rare “phase runs”, - monotonic changes over several linear periods by large values which can significantly exceed 2π .

4.3 Steady state solutions.

Steady power-law solutions of WKE which correspond to a direct cascade of energy and an inverse waveaction cascade are,

$$n(k) = C_1 P^{1/3} k^{-4} \quad (21)$$

$$n(k) = C_2 Q^{1/3} k^{-23/6}, \quad (22)$$

where P and Q are the energy and the waveaction fluxes respectively and C_1 and C_2 are constants, and $k = |\mathbf{k}|$. The first of these solutions is the famous ZF spectrum [8] and it has a great relevance to the small-scale part of the sea surface turbulence. It has been confirmed in a number of recent numerical works [1–3], but we will also confirm it in our simulation.

Now, let us consider the steady state solutions for the one-mode PDF. Note that in the steady state $\gamma/\eta = n$ which follows from WKE (20). Then, the general steady state solution to (14) is

$$P = \text{const} \exp(-s/n) - (F/\eta) Ei(s/n) \exp(-s/n), \quad (23)$$

where $Ei(x)$ is the integral exponential function. At the tail $s \gg n_k$ we have

$$P \rightarrow -\frac{F}{s\gamma} \quad (24)$$

if $F \neq 0$. The $1/s$ tail decays much slower than the exponential (Rayleigh) part and, therefore, it describes strong intermittency. On the other hand, $1/s$ tail cannot be infinitely long because otherwise the PDF would not be normalisable. As it was argued in [5], the $1/s$ tail should with a cutoff because the WT description breaks down at large amplitudes s . This cutoff can be viewed as a wavebreaking process which does not allow wave amplitudes to exceed their critical value, $P(s) = 0$ for $s > s_{nl}$.

Relation between intermittency and a finite flux in the amplitude space was observed numerically also for the Majda-Mc-Laughlin-Tabak model by Rumpf and Biven [21].

4.4 Nonlinear frequency shift.

WT theory predicts that the lowest-order effect of small nonlinearity of the wave system will be a shift in frequency,

$$\omega_{NL}(\mathbf{k}) = 2 \sum_j |W_{jk}^{jk}|^2 n_j. \quad (25)$$

Strictly speaking, each mode is shifted by $2 \sum_j |W_{jk}^{jk}|^2 A_j^2$ where as expression (25) represents the mean of this quantity. However, this mean is much greater than r.m.s. fluctuations of this quantity, i.e. ω_{NL} is approximately equal to its mean. This can be seen by splitting the j -sum onto such sub-sums that W does not vary much within each sub-sum. Then, we take into account independence of A_j^2 for different j 's and apply the central limit theorem.

Expression (25) appears to diverge at low k on the ZF spectrum (21) which means that the frequency shift will be dominated by the spectrum near the low- k cutoff, i.e. near the forcing scales. On the other hand, the discreteness effects are most felt at low wavenumbers and, therefore, we may expect some departure in the numerical values of the frequency shift from the theoretical prediction based on the continuous k -space. In reality, we observe even more dramatic qualitative differences and, instead of just one shifted frequency peak we observe 2 peaks at each wavenumber, - one shifted and another with un-shifted (i.e. linear) frequency.

5 Resonant interaction in discrete k -space

Nonlinear wave interactions crucially depend on the sort of resonances the dispersion relation allows. The dispersion relation of the surface gravity waves is concave and hence it forbids three-wave interactions, so that the dominant process is four-wave. Resonant manifold is defined by resonant conditions $\mathbf{k} + \mathbf{k}_1 = \mathbf{k}_2 + \mathbf{k}_3$, $\omega_{\mathbf{k}} + \omega_{\mathbf{k}_1} = \omega_{\mathbf{k}_2} + \omega_{\mathbf{k}_3}$ or, substituting $\omega_{\mathbf{k}} = \sqrt{gk}$,

$$\begin{aligned} \mathbf{k} + \mathbf{k}_1 &= \mathbf{k}_2 + \mathbf{k}_3 \\ \sqrt{k} + \sqrt{k_1} &= \sqrt{k_2} + \sqrt{k_3} \end{aligned} \quad (26)$$

While in the continuous k -space resonant conditions are invariant with respect to rotations and scaling, that is not true on the wavenumber grid used in numerics. The surviving exact resonances in discrete k -space were studied and classified by Kartashova [22]. However, her statement that (26) has only *mirrored* solutions, i.e. of the form $k = k_2, k_1 = k_3$ (or $k = k_3, k_1 = k_2$), is incorrect. Examples of asymmetric quartets are: $\mathbf{k} = (-20, 15)$, $\mathbf{k}_1 = (-20, -15)$, $\mathbf{k}_2 = (-49, 0)$, $\mathbf{k}_3 = (9, 0)$ or $\mathbf{k} = (-4, 0)$, $\mathbf{k}_1 = (49, 0)$, $\mathbf{k}_2 = (9, 0)$, $\mathbf{k}_3 = (36, 0)$.

To emphasize the importance of different types of resonances, we will first define two main types, - (i) symmetric quartets that transport energy across the angles but not the scales and which are of the form $k = k_2, k_1 = k_3$ (or $k = k_3, k_1 = k_2$), and (ii) asymmetric quartets that transport energy across both the angles and the scales for which $k \neq k_j$, ($j=2,3$). An important subtype of asymmetric

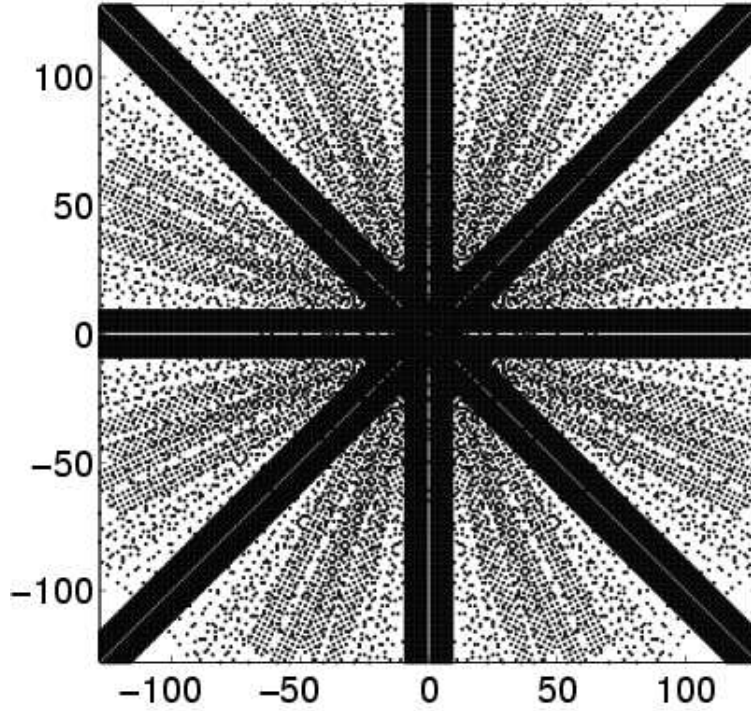


Figure 1: all resonant quartets in which at least one mode is in $k \in [6, 9]$ (a region where waves are forced in our numerical experiments).

resonances is so called the Phillips “figure 8” curve [23] for which $\mathbf{k} = \mathbf{k}_1$, $k \neq k_j (j = 2, 3)$ i.e. they satisfy resonant conditions $2\mathbf{k} = \mathbf{k}_2 + \mathbf{k}_3$, $2\omega_{\mathbf{k}} = \omega_{\mathbf{k}_2} + \omega_{\mathbf{k}_3}$. Their importance lies in the fact that they are the most common asymmetric resonances on our square grid and hence play significant role in energy cascades.

A detailed numerical study of the exact resonances of the surface gravity waves can be found in [24]. Observations of [24] can be briefly summarized as follows. There is much more symmetric quartets than asymmetric ones which means that more resonances carry energy across the angles than across the scales. This property tends to reinforce the wave spectrum isotropy as we indeed observe in our numerics. However, the rate of such an isotropization is directionally dependent since most resonances (particularly the symmetric ones) are concentrated along straight lines parallel to the axes and diagonal to them. An example of this is given in figure 1 which shows all resonant quartets in which at least one mode is in $k \in [6, 9]$ (a region where waves will be forced in our numerical experiments). One can see a characteristic “Union Jack” flag pattern with prominent vertical, horizontal and diagonal stripes as we discussed above. The majority of asymmetric resonances appear to consist of colinear modes and the large portion of them are “figure 8”. These kind of quartets can transfer energy between the scales but they do not participate in the isotropization. Curiously, in colinear “figure 8” quartets one

has $\mathbf{k}_2 = -\frac{1}{4}\mathbf{k}$ and $\mathbf{k}_3 = \frac{9}{4}\mathbf{k}$ which reduces the set of such resonances to the ones where $\mathbf{k} = \mathbf{k}_1$ have components divisible by four.

Because of nonlinearity, the wave resonances have a finite width. Even though this width is small in weakly nonlinear systems, it may be sufficient for activating new mode interactions on the k -space grid and thereby trigger the turbulent cascade through scales. Such quasi-resonances can be roughly modelled through $\mathbf{k}_1 + \mathbf{k}_2 = \mathbf{k}_3 + \mathbf{k}_4$, $|\omega_{\mathbf{k}_1} + \omega_{\mathbf{k}_2} - \omega_{\mathbf{k}_3} - \omega_{\mathbf{k}_4}| < \delta$, where δ describes the resonance broadening. Figure 2 shows quasi-resonant generations of modes on space $[-64, 64]^2$, where initially (generation 1) only modes in the ring $6 < k < 9$ were present (as in our numerical experiment). With broadening of the resonant manifold smaller than the critical $\delta_{crit} \sim 1.4 * 10^{-5}$, a finite number of modes outside the initial region get excited due to exact resonances (generation 2) but there are no quasi-resonances to carry energy to outer regions in further generations. If broadening is larger than critical, energy cascades infinitely. Contrary to the the case of capillary waves where quasi-resonant cascades die out if broadening is not large enough [25], in the case presented here quasi-resonant cascades either do not happen at all (if $\delta < \delta_{crit}$) or they spread through the wavenumber space infinitely (if $\delta > \delta_{crit}$), as happens on Figure (2).

6 Numerical simulation

Numerical simulations presented in this work were performed on a single-processor workstation (2.5GHz, 1Gb RAM). We performed a direct numerical simulation, integrating the dynamical equations of motion (4) and (5) using pseudo-spectral method with resolution of 256×256 wavenumbers. Numerical integrator used for advancing in time was RK7(8) presented in [26]. Time step was $\frac{T_{min}}{35}$ where T_{min} is the period of the shortest wave on the axis. Approximate processor time for this work was 4.5 weeks.

In our numerical experiment, we force the system in the k -space ring $k_* < k < k^*$ with $k_* = 6$ and $k^* = 9$. This ring is located at the low wavenumber part of the k -space in order to generate energy cascade toward large k 's, but we deliberately avoid forcing even longer waves ($k < 6$) because our experience shows that this would lead to undesirable strong anisotropic effects. In the ring, we fix the amplitude at the expected statistical steady state of the wave spectrum, $\langle |a_{\mathbf{k}}(t)|^2 \rangle \sim k^{-4}$, and hence we set $|\eta_{\mathbf{k}}| \sim k^{-7/4}$, $|\Psi_{\mathbf{k}}| \sim k^{-9/4}$. These fixed amplitudes were then multiplied by random phase factors. Thus, surface $\eta_{\mathbf{k}}$ and velocity potential $\Psi_{\mathbf{k}}$ were set to $2\pi^3 e^{i\theta_{\mathbf{k}}} * k^{\alpha_{\mathbf{k}}}$, where $\theta_{\mathbf{k}}$ were uniformly distributed in $[0, 2\pi]$ and

$$\alpha_k = x \left\{ \begin{array}{ll} \left[1 + \left(\frac{k_* - k}{k^*} \right)^2 \right]^{3/4} & \text{if } k \in (0, k_*) \\ 1 & \text{if } k \in [k_*, k^*] \\ \left(\frac{k}{k^*} \right)^{3/4} & \text{if } k \in (k^*, \frac{N}{2}) \end{array} \right\}$$

where $x = -7/4$ for the surface and $x = -9/4$ for velocity potential. Damping was applied in both small and large wavenumber regions. Since both the energy and the number of particles are conserved in four-wave systems, there are two cascades being formed to achieve a steady state: a *direct* cascade

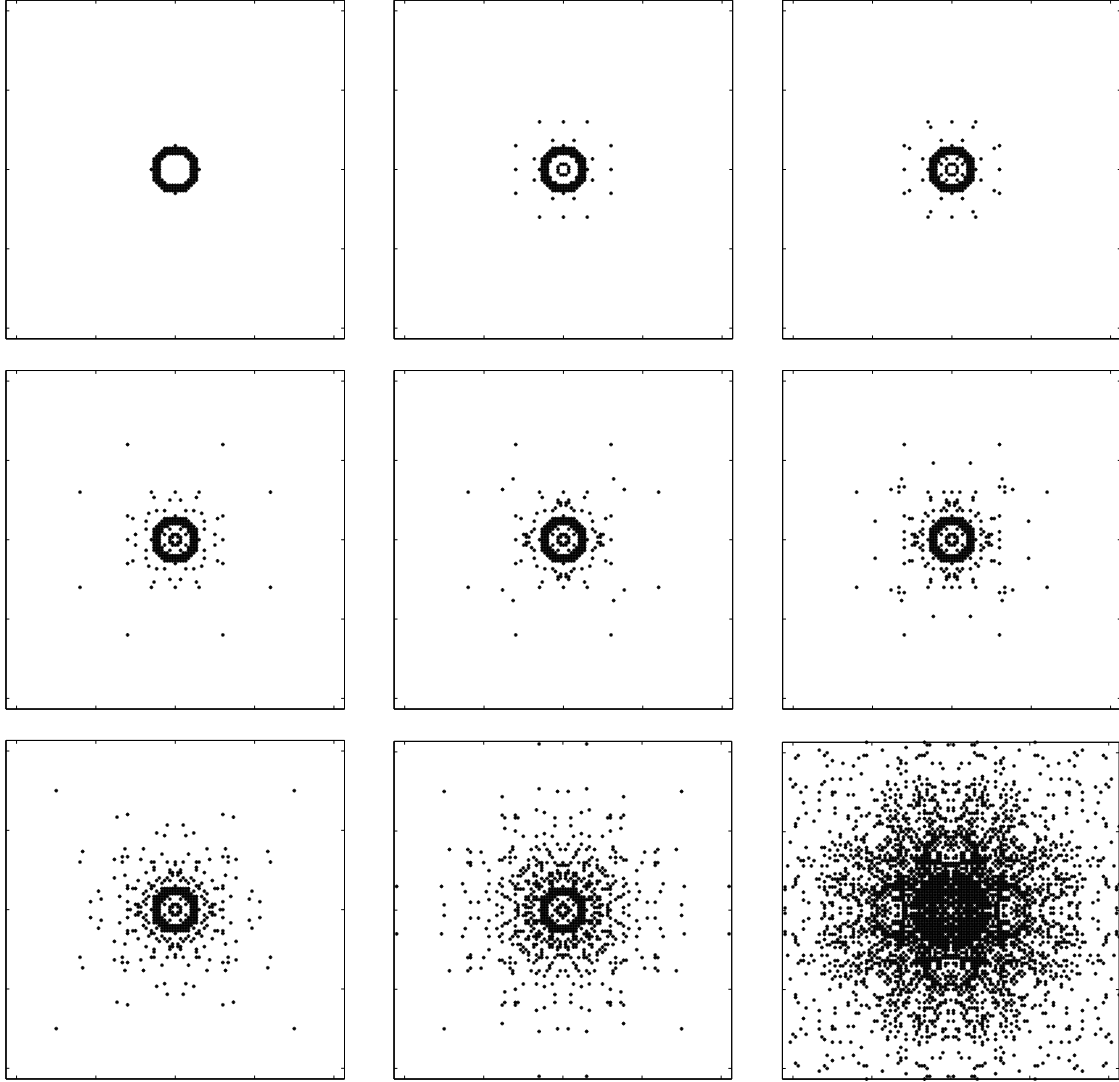


Figure 2: Quasi-resonant generations of modes on space $[-64, 64]^2$, where initially (generation 1) only modes in the ring $6 < k < 9$ were present. Here the value of the broadening is slightly above δ_{crit}

of energy toward higher wave numbers and an *inverse* cascade of particles. This inverse cascade leads to the formation of a *condensate*: a large amplitude wave with minimal possible wave number. Such a condensate may non-locally interact with other parts of the spectrum. Since in the present work we concentrate our attention on the direct cascade, we “remove” the condensate by using adaptive damping. Note that the condensate has the minimum wave number, therefore it “feels” the discreteness of numerical grid in the strongest possible way.

At large wavenumbers, damping is needed to absorb the energy cascade and, therefore, to avoid “bottleneck” spectrum accumulation near the cutoff wavenumber. In our simulations, we implemented the damping as a low-pass filter $\gamma_{\mathbf{k}}$ applied to the k -space variables at each timestep. The damping function had the form

$$\gamma_{\mathbf{k}} = \left\{ \begin{array}{ll} 5(k-6)^{3/2} & k < 6 \\ 0 & k \in [6, 64] \\ 0.028(k-64)^2 & k > 64 \end{array} \right\}$$

Nonlinearity parameter was set to $\varepsilon = 2 \cdot 10^{-2}$, which is a sufficient value to produce a resonance broadening for supporting energy cascade.

7 Results

7.1 Spectrum

Measuring the spectrum has by far dominated WT studies because this is the most basic and robust theoretical object and because this quantity is easier to observe experimentally than more subtle statistical quantities. For the surface gravity waves, the WT prediction about the energy cascade spectrum have been confirmed in several recent numerical studies [1–3]. Here, we also start by presenting the spectrum. Figure 3 shows the spectrum at an early time and at $t = 2000T_p$, where T_p is period of the slowest mode ($k = 10$). The obtained spectrum is in agreement with the predictions of WT theory in the inertial range as it is very close to the k^{-4} shape of the ZF spectrum. Our subsequent statistical measurements will be made at the time where this steady state spectrum has already got established.

7.2 Wave-amplitude probability density function and its moments

Now we consider the PDF of amplitudes for which predictions were made recently within the WT approach. To measure the PDF of amplitudes $|a_{\mathbf{k}}(t)|^2$, we set two radial regions in \mathbf{k} -space $k_{15} = [13, 17]$, and $k_{35} = [33, 37]$. These regions were inside the inertial range and had well mixed phases and amplitudes since the experiment was done after performing 2000 rotations of the peak mode. We looked at the time-span of approximately 855 rotations of modes $k = 15$ or 1230 rotations of modes $k = 35$ and collected amplitudes of all modes from these three regions. The number of amplitudes collected was over 1.1 million in region k_{15} and over 2.1 million in region k_{35} .

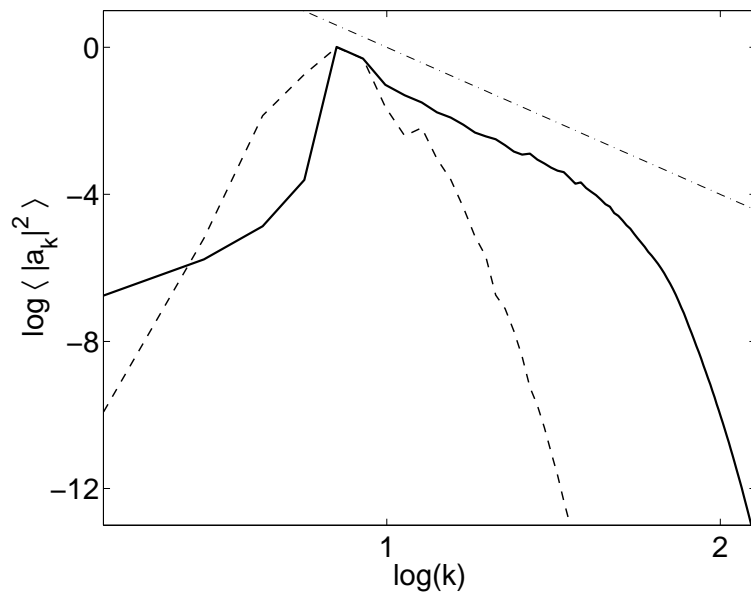


Figure 3: One-dimensional energy spectrum of waves. Solid line shows the late-time quasi-steady spectrum, whereas the dashed line represents an early-time spectrum. The straight line corresponds to the theoretical WT prediction (-4 slope). Here Log is base 10.

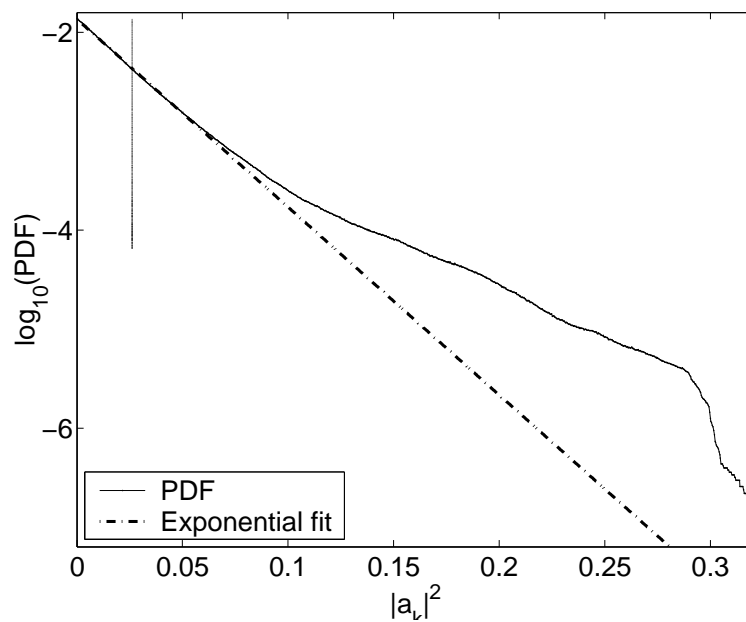


Figure 4: Probability density function for the amplitude $|a_k|^2$ with $k \in [13, 17]$. The linear fit is shown based on the slope of the low-amplitude part (the Gaussian core). The vertical straight line marks the mean value (spectrum) $n_k = \langle |a_k|^2 \rangle$.

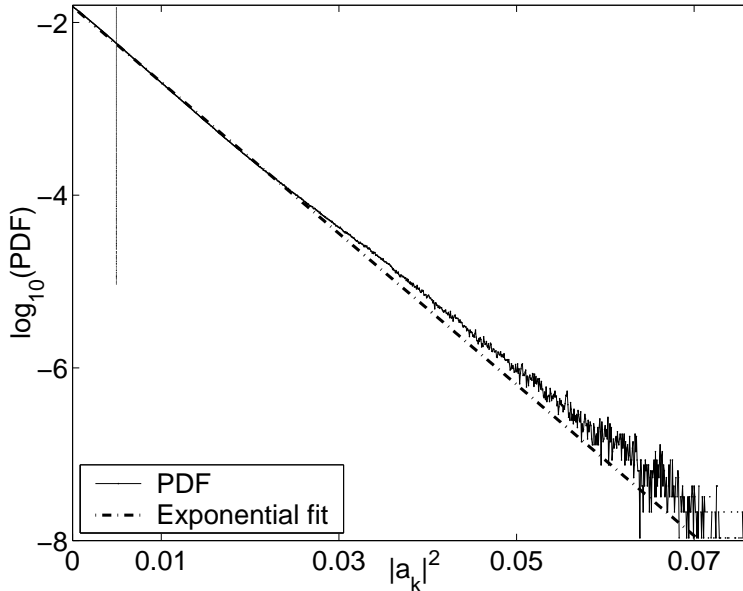


Figure 5: Probability density function for the amplitude $|a_k|^2$ with $k \in [33, 37]$. Same notations as in Figure 4.

Figure 4 shows a log-plot of the PDF the amplitude A_k^2 in k_{15} and an exponential fit of its low-amplitude part. One can see intermittency, i.e., an anomalously large probability of strong waves. We can also see that this discrepancy from Gaussianity happens in the tail, i.e. well below the mean amplitude value $s = n_k$. While the PDF tail is not long enough for drawing decisive conclusions about realization of the theoretically predicted $1/s$ scaling, it certainly gives a conclusive evidence that the probabilities of large amplitudes are orders of magnitude higher than in Gaussian turbulence. Figure 5 shows the PDF of A_k^2 in k_{35} . We can see some non-Gaussianity in k_{35} as well, although much less than in k_{15} . Similar conclusion that the gravity wave turbulence is more intermittent at low rather than high wavenumbers was reached on the basis of numerical simulations in [3].

Deviations from Gaussianity can be also seen in figure 6 which shows ratio of the moments $M^{(p)} = \langle |a|^{2p} \rangle$ to their values in Gaussian turbulence, $n p!$. Again, we can see that such deviations are greater at the small- k part of the inertial range.

7.3 Frequency properties.

The lowest order nonlinearity effect in WT of the surface gravity waves was predicted to be the nonlinear frequency shift of the wave modes. We examine this prediction by performing the time-Fourier transform at each fixed wavenumber. Two typical plots, for $\mathbf{k} = (17, 0)$ and $\mathbf{k} = (31, 0)$, are shown in Figures 7 and 8 respectively. In striking contrast with WT expectations, we always see two peaks - the bigger

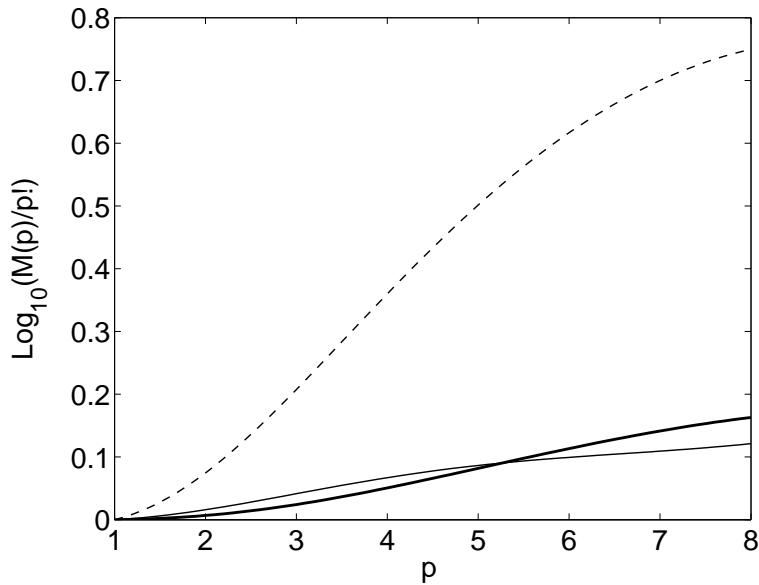


Figure 6: Ratio of the moments $M^{(p)} = \langle |a|^{2p} \rangle$ to their values in Gaussian turbulence, $n p!$, for $k \in [13, 17]$ (dashed line), $k \in [23, 27]$ (thin solid line) and $k \in [33, 37]$ (thick solid line).

and thinner one is exactly at the linear frequency and a smaller and wider peak at a shifted frequency. We interpret the second peak is a nonlinear effect since there is no frequency shift in the linear system. It is interesting that this frequency shift is different from the one predicted by WT and, particularly, it has different sign. The ratio of the frequency shift predicted by WT, ω_{NL} , to the distance between the two peaks is shown in in Figure 9 where one could observe a close to linear law. The distance between the two peaks is also significantly less in magnitude than ω_{NL} , which could possibly be explained by weakening of the nonlinear interaction due to loss of resonant quartets in discrete k -space with respect to the continuous k -space.

Also, it appears that the ratio of squares of the peak frequencies is approximately equal to 2 for all wavenumbers, see figure 10 (i.e. the second peak oscillates with the linear frequency of mode whose wavenumber is twice the one of the first mode). These dependencies, and the nature of the second peak itself, remain to be explained. The two-frequency character at each wavenumber has an interesting relation to the amplitude and phase dynamics as will be seen in the next section.

7.4 Amplitude and phase evolution.

Figures 11 and 12 show time evolution of the amplitude A_k and the (interaction representation) phase ϕ_k respectively for $\mathbf{k} = (17, 0)$. We zoom in at the amplitude fluctuations in figure 13, where one can see large-amplitude quasi-periodic oscillations on A_k , - it changes in value several-fold over a time

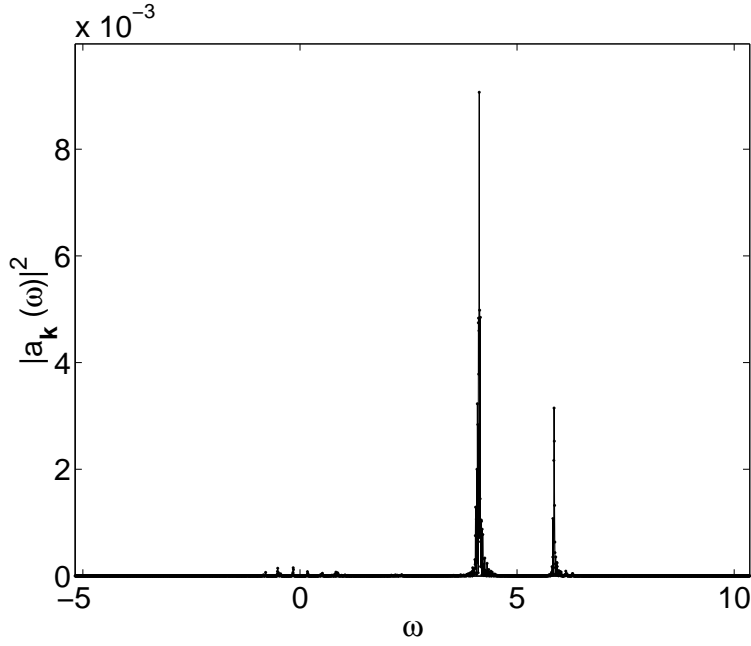


Figure 7: Frequency distribution of waveaction at a fixed wavenumber $\mathbf{k} = (17, 0)$.

comparable to the linear wave period. This indicates that nonlinearity is not weak, otherwise the amplitude changes would be slower than the linear oscillations. The phase evolution seen in figure 12 consists of the time intervals when it oscillates quasi-periodically (with amplitude less than 2π) which are inter-leaved by sudden “phase runs”, - fast monotonic phase changes by values which can significantly exceed 2π . By juxtaposing figures 11 and 12, one can see that when the phase runs happen then the amplitude is close to zero. Note that such observed behaviour of the phase is very different from a simple WT prediction that its mean value grows with the rate ω_{NL} and that the r.m.s. fluctuations of this quantity grow as a square root of time [5].

These observations, together with the two-peak character of the time-Fourier spectrum, suggest that at each wavenumber \mathbf{k} there are two modes:

$$a_k = c_1 + c_2 e^{-i\omega^* t},$$

where $\omega^* > \omega_k$ and the complex amplitudes are c_1 and c_2 varying in time slower than the linear oscillations. Most of the time $|c_1| > |c_2|$ and, therefore, the phase ϕ_k oscillates periodically about the some mean value (equal to the phase of c_1). However, sometimes c_2 becomes greater than c_1 and then the path of a_k will encircle zero in the complex plane, so that ϕ_k starts gaining 2π for each rotation. These are the phase runs, and in order to trigger these runs a_k must cross zero, which explains the observed small values of this quantity during the phase runs.

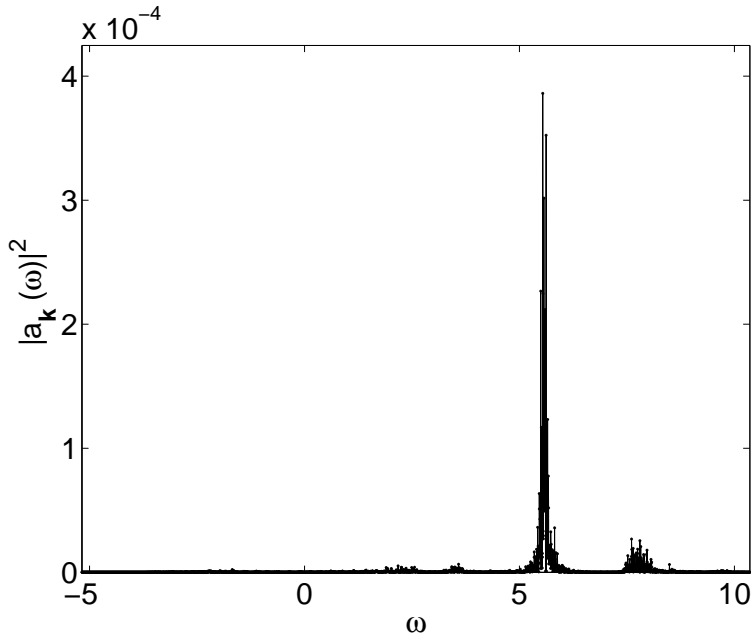


Figure 8: Frequency distribution of waveaction at a fixed wavenumber $\mathbf{k} = (31, 0)$.

In figure 15 we show comparison of the mean rate of the phase change during the upward phase runs and the second peak's frequency at different wavenumbers. A significant coincidence of these two curves supports the proposed above two-mode explanation.

A word of caution is due about the simple two-mode explanation of the phase runs. Indeed, according to this picture the phase should always run to higher values whereas in figure 12 we see both upward and downward runs. A possible explanation of this is that phase runs may be triggered not only by sharp peaks but also by broadband distributions with frequencies less than the linear one. Such broadband distributions could be made of modes which are strong (and therefore can produce phase runs) but whose duration in time is short and sporadic and at different frequencies (hence a broad spectrum). This picture is supported by the fact that the amount of total wave energy in the frequency range below the linear frequency is similar (and for low wavenumbers even greater) than the amount of energy in the range above the linear frequencies, see figure 17. Evidence of relation of the sub-linear modes and the downward phase runs is shown in figure 16 where the mean rate of the phase change during the downward phase runs and the frequency of the highest sub-linear peak. Again, we can see agreement of these two curves although with a greater level of fluctuations due to the fact the sub-linear modes are very spread over different frequencies.

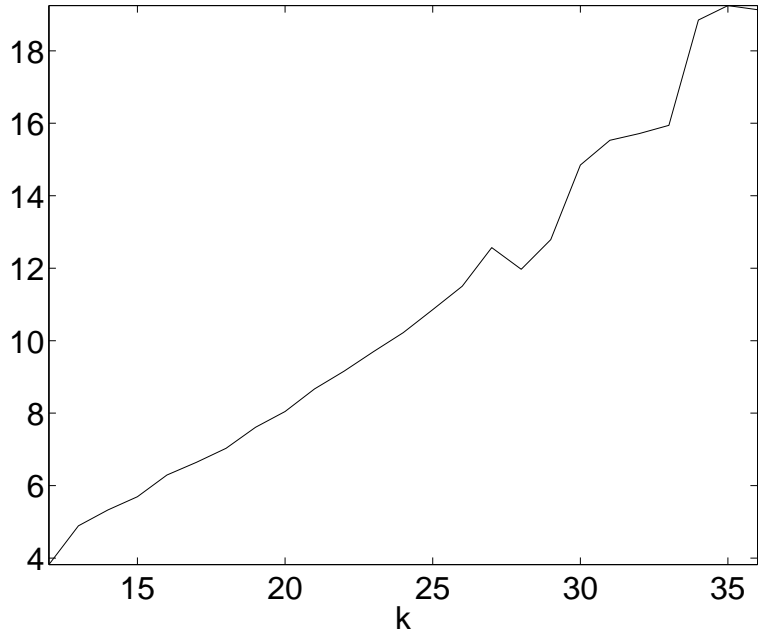


Figure 9: Ratio of the nonlinear frequency shift to the distance between two frequency peaks, for different wavenumbers.

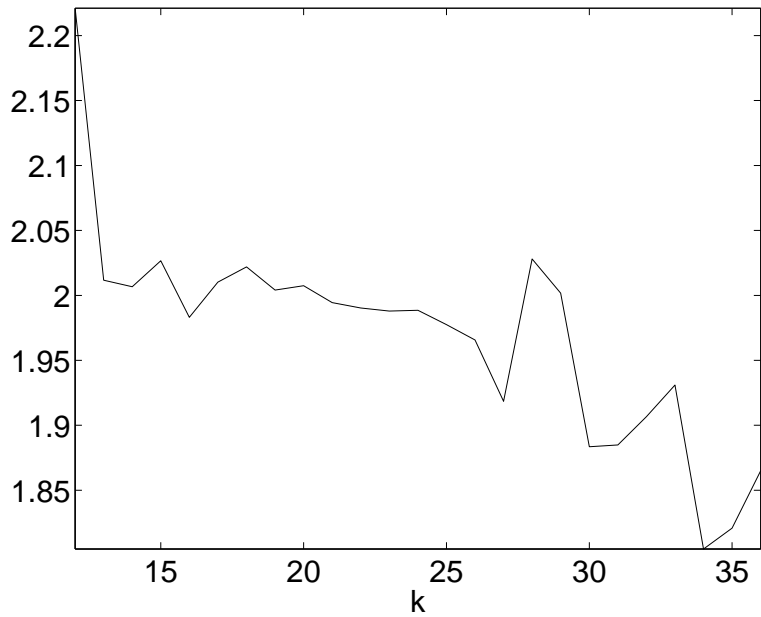


Figure 10: Ratio of squares of the peak frequencies for different wavenumbers.

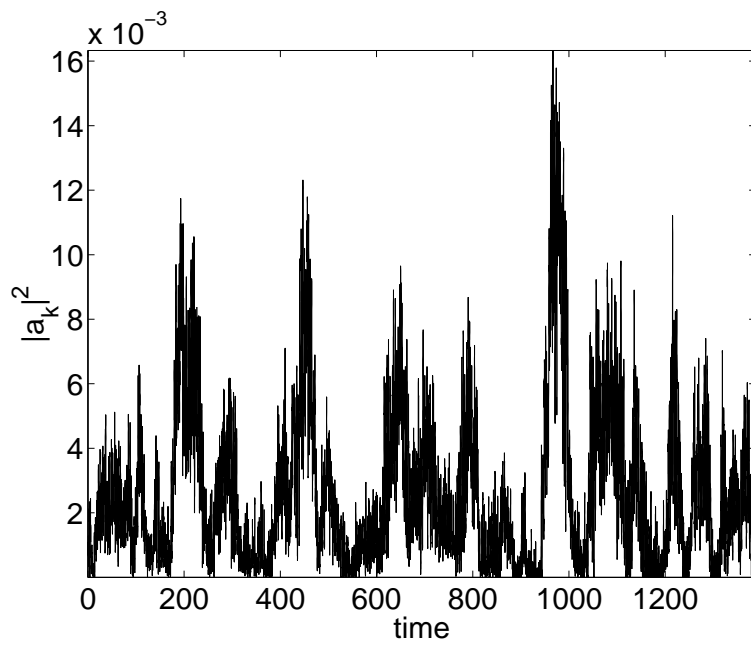


Figure 11: Graph of $A_k^2(t)$ at wavenumber $\mathbf{k} = (25, 0)$.

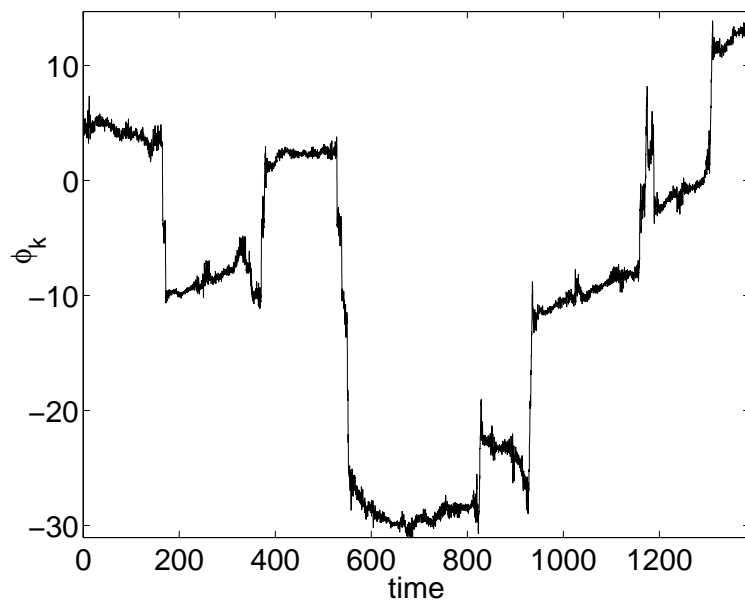


Figure 12: Phase evolution, $\phi_k(t)$, at wavenumber $\mathbf{k} = (25, 0)$.

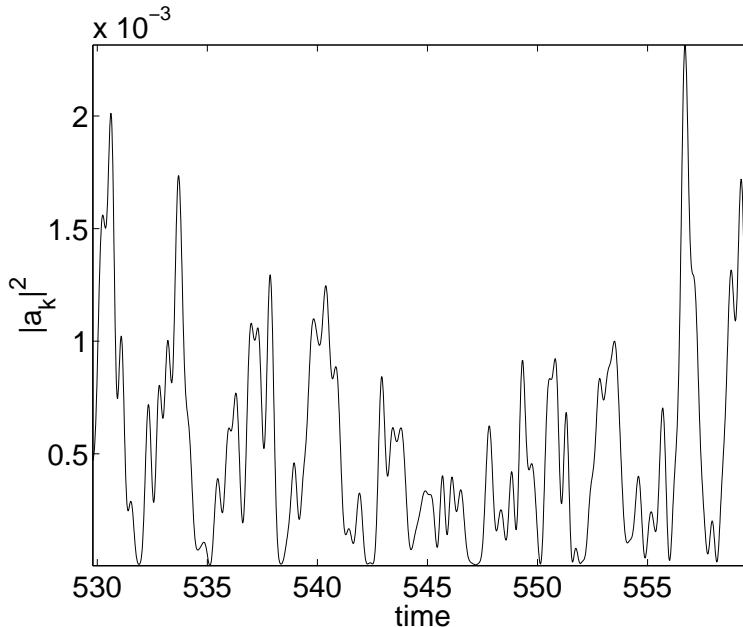


Figure 13: Detailed graph of $A_k^2(t)$ at wavenumber $\mathbf{k} = (25, 0)$.

7.5 Nonlinearly active modes and cascade “avalanches”

Component with the shifted frequency ω^* is clearly a nonlinear effect (there is no frequency shift in linear dynamics). Thus, the relative strength of c_2 and c_1 can be used as a measure of nonlinearity. Particularly, the phase runs mark the events when nonlinearity becomes strong. Figure 14 shows locations of the phase runs in the 2D wavenumber space which happened at $t = 500$. Note that at that time ZF steady spectrum has already formed. In the energy cascade range, we see that the phase run density is increasing toward high k 's, which is in agreement with the WT prediction that the nonlinearity grows as one cascades down-scale [10, 11]. Curiously, we also observe high density of the phase runs within the circle $k < 6$, which is, perhaps, manifestation of a waveaction accumulation via an inverse cascade process. However, this range is too small for any meaningful conclusions to be made about the inverse cascade properties.

The energy cascade from the forcing region toward the high wavenumber region proceeds in a non-uniform in time fashion somewhat resembling sporadic sandpile avalanches. This arises due to the k -grid discreteness effects which tend to block the resonant wave interaction when the wave intensities are small. This situation resembles “frozen turbulence” of [13]. Thus, the wave energy does not cascade to high wavenumbers and it tends to accumulate near the forcing scales until the wave intensity is strong enough to restore the resonant interaction via the nonlinear resonance broadening. At this moment the energy cascade toward high wavenumbers sets in, and this leads to depletion of energy at the forcing

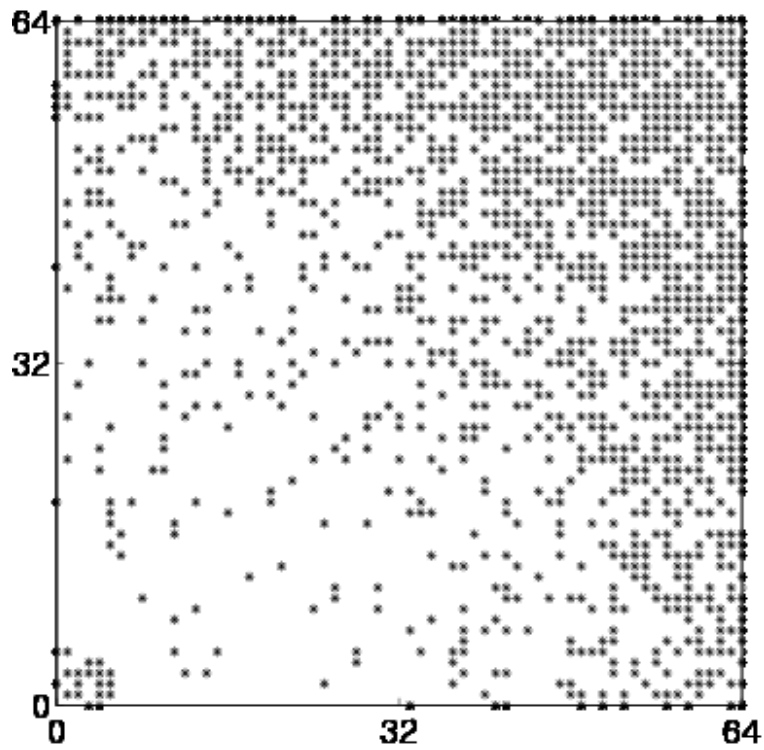


Figure 14: Phase runs detected in the 2D wavenumber grid over the time period.

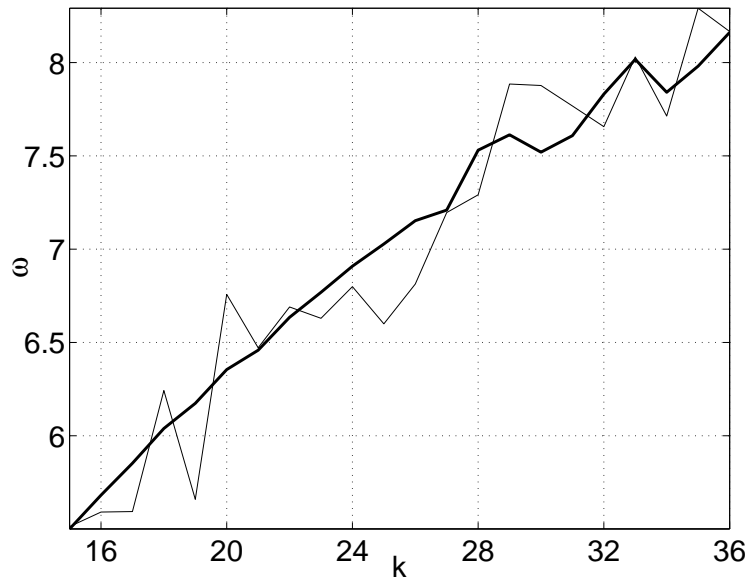


Figure 15: Mean rate of the phase change during the upward phase runs (thin curve) and the second peak's frequency (thick curve) as functions of wavenumber.

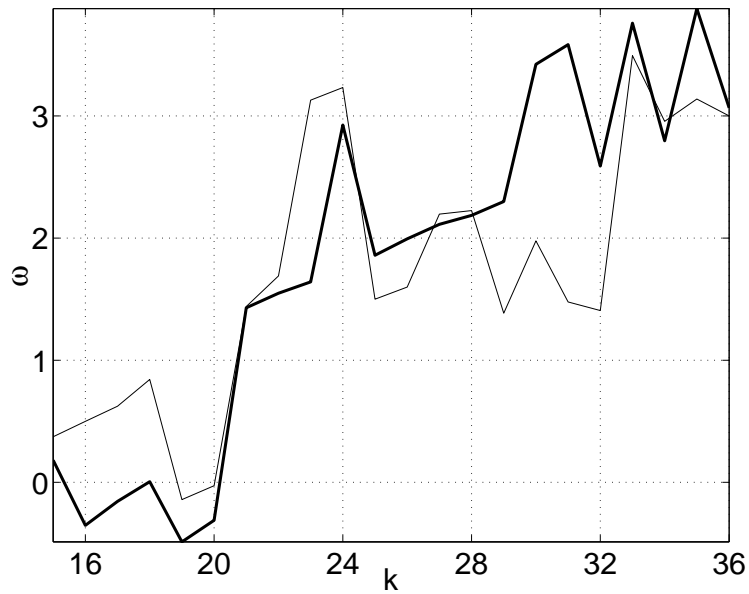


Figure 16: Mean rate of the phase change during the downward phase runs (thin curve) and the frequency of the highest sub-linear peak (thick curve) as functions of wavenumber.

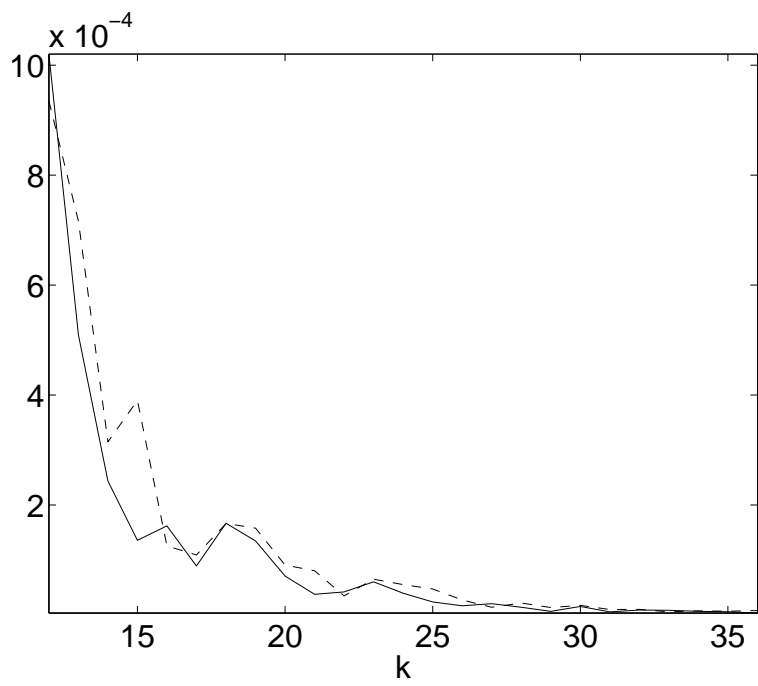


Figure 17: Total power of modes with frequencies below the linear frequency (solid line) and the modes with frequencies above the linear frequency (dashed line).

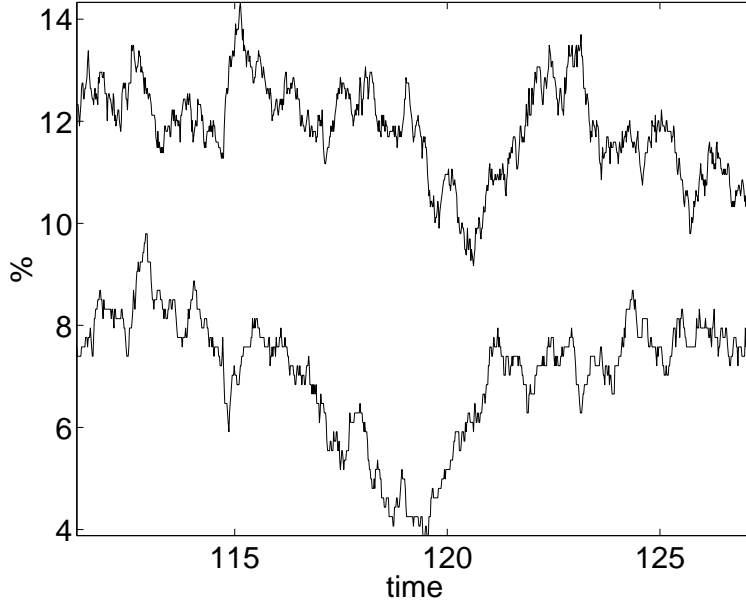


Figure 18: Percentage of modes experiencing phase runs in the range $13 < |k| < 29$ (lower curve) and in the range $30 < |k| < 45$ (upper curve).

scale, - “sandpile tips over”. In turn, depletion of energy at the forcing scale leads to blocking of the energy cascade, and the process continues in a repetitive manner. As a result system oscillates between the state of “frozen turbulence” and the state of “avalanche cascade”. This behaviour is illustrated in figure 18 which shows percentage of modes experiencing phase runs in two different wavenumber ranges $13 < k < 29$ and $30 < k < 45$. One can see that the shapes of these two curves bear a great degree of similarity up to a certain time delay and a vertical shift in the second curve with respect to the first one. The vertical shift reflects the fact that the energy cascade gets stronger as it proceeds to large wavenumbers. The time delay, on the other hand indicates the direction and the character of the sporadic energy cascade. It shows that a higher (lower) nonlinear activity at low k 's after a finite delay causes a higher (lower) activity at higher k 's, which could be compared with propagation of an avalanche (quenching) down a sandpile.

7.6 Correlations of phases, phase factors and amplitudes.

WT closure relies on the RPA properties of the wave fields, i.e. that the amplitudes A_k and the phase factors ψ_k are statistically independent variables. On the other hand, WT calculation for the phases ϕ_k shows that these quantities get correlated. In order to check these properties and predictions numerically, let us introduce a function that measures the degree of statistical dependence (or independence)

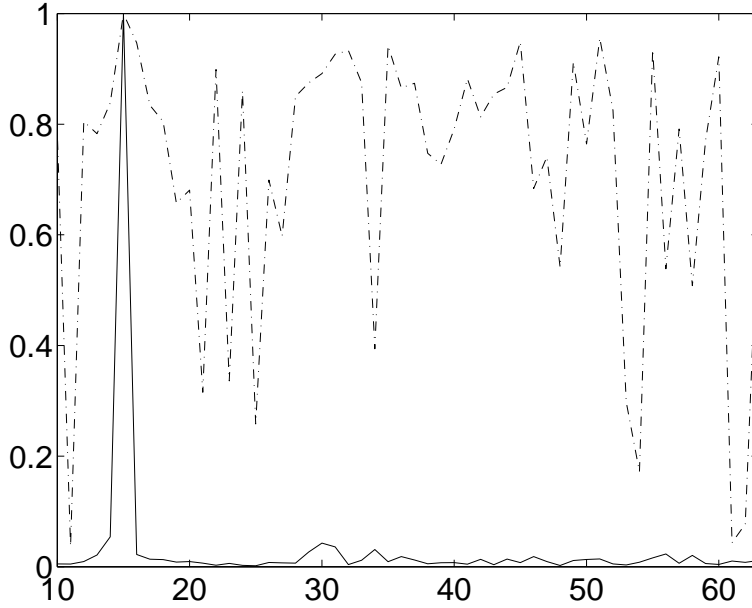


Figure 19: Two-point auto-correlations for phases ϕ_k (dashed line) and phase factors $\psi_k = e^{i\phi_k}$ (solid line) with one point fixed at $\mathbf{k} = (15, 0)$.

of some Fourier-space variables $X(\mathbf{k}_1)$ and $Y(\mathbf{k}_2)$,

$$\mathcal{C}_{X,Y}(\mathbf{k}_1, \mathbf{k}_2) = \frac{\langle X(\mathbf{k}_1)Y(\mathbf{k}_2) \rangle - \langle X(\mathbf{k}_1) \rangle \langle Y(\mathbf{k}_2) \rangle}{\sqrt{\langle X^2(\mathbf{k}_1) \rangle - \langle X(\mathbf{k}_1) \rangle^2} \sqrt{\langle Y^2(\mathbf{k}_2) \rangle - \langle Y(\mathbf{k}_2) \rangle^2}}. \quad (27)$$

For example, we can examine to what degree amplitudes A and independent of the phase factors ψ by looking at the function $\mathcal{C}_{A,\psi}(\mathbf{k}_1, \mathbf{k}_2)$ for different values of \mathbf{k}_1 and \mathbf{k}_2 . Independence of the amplitudes at different wavenumbers can be examined by the auto-correlation function $\mathcal{C}_{A,A}(\mathbf{k}_1, \mathbf{k}_2)$, and similar for the phase factors and the phases. We restrict ourselves with choosing $\mathbf{k}_1 = (15, 0)$ and $\mathbf{k}_2 = (k, 0)$ with $k \in (10, 64)$. Figure 19 shows the values of correlators $\mathcal{C}_{\phi,\phi}(\mathbf{k}_1, \mathbf{k}_2)$ and $\mathcal{C}_{\psi,\psi}(\mathbf{k}_1, \mathbf{k}_2)$ as functions of k . In agreement with WT predictions, auto-correlations of ψ_k 's are very small whereas the ones of ϕ_k 's are significant (except, of course, for $k = 15$ where by definition these correlators are equal to one). Correlators $\mathcal{C}_{A,A}(\mathbf{k}_1, \mathbf{k}_2)$ and $\mathcal{C}_{A,\psi}(\mathbf{k}_1, \mathbf{k}_2)$ are shown in figure 20. Again, we see a good agreement with the WT prediction: these correlations are very small (except, again, $\mathcal{C}_{A,A}(15, 15) = 1$).

8 Discussions

In this paper, we used direct numerical simulations of the free water surface in order to examine the statistical properties of the water-wave field beyond the energy spectrum. Our first aim was to

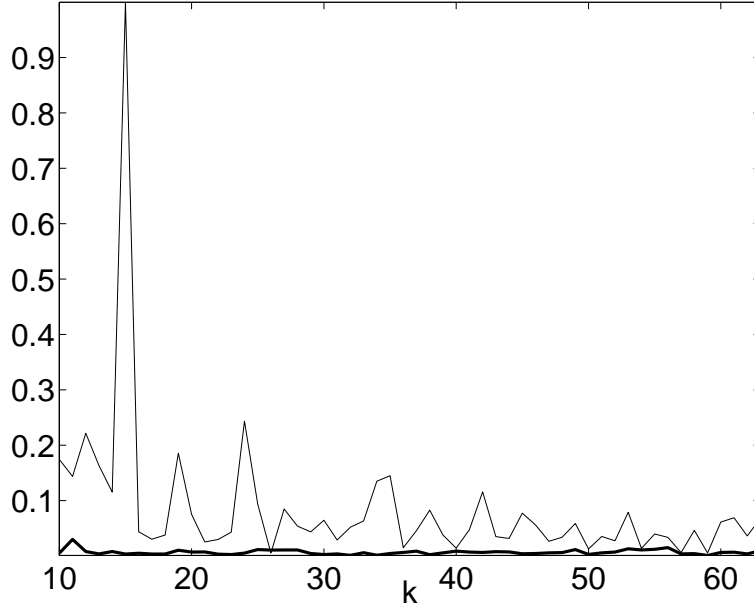


Figure 20: Two-point auto-correlation of amplitudes A_k (thin curve) and two-point correlation between A_k and phase factors ψ_k (thick curve) with one point fixed at $\mathbf{k} = (15, 0)$.

check recent predictions of the WT theory about the PDF and intermittency, about the character of correlations of the wave amplitudes and phases, as well as older predictions about the nonlinear frequency shift. We particularly focused on the question how the effects of discreteness and finite nonlinearity change statistics with respect to the WT closure developed for weak nonlinearities and for a continuous wavenumber space.

Firstly, following [1–3] we confirm formation of the Zakharov-Filonenko spectrum predicted by WT. Secondly, we measured PDF for the wave amplitudes and observe an anomalously large, with respect to Gaussian fields, probability of strong waves. This result is in agreement with recent theoretical predictions of [4, 5]. Thirdly, we measure correlations for the amplitudes, phases and phase factors and we observe agreement with predictions of [4, 5]. Namely, the amplitude and the phase correlations behave as statistically independent variables, whereas the phases develop strong auto-correlations over the nonlinear time. Note that these properties are fundamental for the WT closure to work, so in a way we provide a numerical validation for the WT approach.

On the other hand, we find discrepancies with some other WT predictions. In particular, we observe deviation from the WT prediction that the wave frequencies are shifted by ω_{NL} given by (25). Instead, we find that at each k there are two sharp frequency peaks: a dominant one at the linear frequency and a weaker one with a frequency shift smaller and of the opposite sign with respect to (25). Somewhat related to this two-peak frequency structure is the observed time behaviour of the phase. Instead of

a gradual growth of the mean phase with rate ω_{NL} and growth of its r.m.s. fluctuations predicted by WT [5], we observe calm periods during which the phase oscillates within 2π -wide margins intermittent with sudden phase runs during which it experiences a monotonic change significantly greater than 2π . Finally, we observe that the energy cascade is “bursty” in time and is somewhat similar to sporadic sandpile avalanches. We give a plausible explanation of this behaviour as an interplay of effects of discreteness and nonlinearity. Because in between of the avalanche discharges the resonances are absent then, at least qualitatively, one can refer to the KAM theory and say that the evolution should remain close to the corresponding integrable case, - the linear system in our case. This scenario can possibly explain the observed absence of the nonlinear frequency shift in the main frequency component.

9 Appendix

9.1 Interaction coefficient for gravity waves

The coefficient of four-wave interactions for gravity waves is given by rather long expression which was first calculated by Zakharov with a minor mistake which was further corrected by Krasitsky, see [20, 27]. The expression reads,

$$\begin{aligned}
W_{mn}^{jl} = & -\frac{1}{16\pi^2} \frac{1}{(k_j k_l k_m k_n)^{1/4}} \{ \\
& - 12k_j k_l k_m k_n \\
& - 2\frac{(\omega_j + \omega_l)^2}{g^2} [\omega_m \omega_n (\mathbf{k}_j \cdot \mathbf{k}_l - k_j k_l) + \omega_j \omega_l (\mathbf{k}_m \cdot \mathbf{k}_n - k_j k_l)] \\
& - 2\frac{(\omega_j - \omega_m)^2}{g^2} [\omega_l \omega_n (\mathbf{k}_j \cdot \mathbf{k}_m + k_j k_m) + \omega_j \omega_m (\mathbf{k}_l \cdot \mathbf{k}_n + k_l k_n)] \\
& - 2\frac{(\omega_j - \omega_n)^2}{g^2} [\omega_l \omega_m (\mathbf{k}_j \cdot \mathbf{k}_n + k_j k_n) + \omega_j \omega_n (\mathbf{k}_l \cdot \mathbf{k}_m + k_l k_m)] \\
& + (\mathbf{k}_j \cdot \mathbf{k}_l + k_j k_l)(\mathbf{k}_m \cdot \mathbf{k}_n + k_m k_n) \\
& + (-\mathbf{k}_j \cdot \mathbf{k}_m + k_j k_m)(-\mathbf{k}_l \cdot \mathbf{k}_n + k_l k_n) \\
& + (-\mathbf{k}_j \cdot \mathbf{k}_n + k_j k_n)(-\mathbf{k}_l \cdot \mathbf{k}_m + k_l k_m) \\
& + 4(\omega_j + \omega_l)^2 \frac{(\mathbf{k}_j \cdot \mathbf{k}_l - k_j k_l)(-\mathbf{k}_m \cdot \mathbf{k}_n + k_m k_n)}{\omega_{j+l}^2 - (\omega_j + \omega_l)^2} \\
& + 4(\omega_j - \omega_m)^2 \frac{(\mathbf{k}_j \cdot \mathbf{k}_m + k_j k_m)(\mathbf{k}_l \cdot \mathbf{k}_n + k_l k_n)}{\omega_{j-m}^2 - (\omega_j - \omega_m)^2} \\
& + 4(\omega_j - \omega_n)^2 \frac{(\mathbf{k}_j \cdot \mathbf{k}_n + k_j k_n)(\mathbf{k}_l \cdot \mathbf{k}_m + k_l k_m)}{\omega_{j-n}^2 - (\omega_j - \omega_n)^2} \}.
\end{aligned}$$

9.2 Self-interaction coefficient

In order to calculate the nonlinear frequency shift that results from “self-interactions” (25), one has to evaluate (28) on the subset of modes $\mathbf{j} = \mathbf{m}$, $\mathbf{l} = \mathbf{n}$. This gives

$$\begin{aligned}
W_{jl}^{jl} &= -\frac{3}{8\pi^2}(k_j k_l)^{3/2} + \frac{1}{2\pi^2}k_j k_l(k_j + k_l) \cos \theta_{jl} - \frac{1}{8\pi^2}(k_j k_l)^{3/2} \cos^2 \theta_{jl} \\
&+ \frac{1}{4\pi^2}(k_j k_l)^{3/2} \left\{ \frac{(\sqrt{k_j} + \sqrt{k_l})^2 (\cos \theta_{jl} - 1)^2}{|\mathbf{k}_j + \mathbf{k}_l| - (\sqrt{k_j} + \sqrt{k_l})^2} - \frac{(\sqrt{k_j} - \sqrt{k_l})^2 (\cos \theta_{jl} + 1)^2}{|\mathbf{k}_j - \mathbf{k}_l| - (\sqrt{k_j} - \sqrt{k_l})^2} \right\}
\end{aligned} \tag{28}$$

where θ_{jl} is the angle between \mathbf{k}_j and \mathbf{k}_l .

9.3 Self-interaction coefficient in one dimension

Finally we will consider a one-dimensional case when $\mathbf{k}_j \parallel \mathbf{k}_l$ then $\cos \theta_{jl} = \pm 1$ depending on whether $\theta_{jl} = 0$ or $\theta_{jl} = \pi$. This case has no direct relation to the main subject of our paper, but we will write corresponding formulae for reference purposes because we believe that it has not been done in literature before.

If $\theta_{jl} = 0$ then

$$W_{jl}^{jl} = -\frac{1}{2\pi^2}(k_j k_l)^{3/2} + \frac{1}{2\pi^2}k_j k_l(k_j + k_l) - \frac{1}{\pi^2}(k_j k_l)^{3/2} \frac{(\sqrt{k_j} - \sqrt{k_l})^2}{|\mathbf{k}_j - \mathbf{k}_l| - (\sqrt{k_j} - \sqrt{k_l})^2}$$

Performing straightforward manipulation, we obtain

$$W_{jl}^{jl} = \frac{1}{2\pi^2}k_j k_l \min \{k_j, k_l\},$$

which is the known form for this interaction coefficient (see e.g. [17] or [28]).

Similarly, if we assume that $\theta_{jl} = \pi$ then

$$W_{jl}^{jl} = -\frac{1}{2\pi^2}(k_j k_l)^{3/2} - \frac{1}{2\pi^2}k_j k_l(k_j + k_l) + \frac{1}{\pi^2}(k_j k_l)^{3/2} \frac{(\sqrt{k_j} + \sqrt{k_l})^2}{|\mathbf{k}_j + \mathbf{k}_l| - (\sqrt{k_j} + \sqrt{k_l})^2}$$

and finally,

$$W_{jl}^{jl} = -\frac{1}{\pi^2}(k_j k_l)^{3/2} - \frac{1}{2\pi^2}k_j k_l(2 \max \{k_j, k_l\} + \min \{k_j, k_l\})$$

References

- [1] A.I. Dyachenko, A.O. Korotkevich, V.E. Zakharov, *Weak turbulence of gravity waves*, JETP Letters, **77**, No. 10, 2003.

- [2] M. Onorato et.al., *Freely decaying weak turbulence for sea surface gravity waves*, Phys.Review L **89** No.14, September 2002.
- [3] N. Yokoyama, *Statistics of Gravity Waves obtained by direct numerical simulation*, JFM **501**, 169-178 (2004).
- [4] Y. Choi, Y.V. Lvov, S. Nazarenko, B. Pokorni, *Anomalous probability of large amplitudes in wave turbulence*, Physics Letters A, **339**, Issue 3-5, p. 361-369 (also on arXiv:math-ph/0404022 v1 & Apr 2004).
- [5] Y. Choi, Y.V. Lvov, S. Nazarenko, *Probability Densities and Preservation of Randomness in Wave Turbulence* Physics Letters A, **332**, 230-238 (2004); *Joint statistics of amplitudes and phases in wave turbulence*, Physica D **201** (2005) 121-149; Y. Choi, Y.V. Lvov, S. Nazarenko; *Wave turbulence*, in "Recent developments in fluid dynamics" 5 (2004), Transworld Research Network, Kepala, India (also on arXiv.org:math-ph/0412045).
- [6] Y. Lvov and S. Nazarenko, *"Noisy" spectra, long correlations and intermittency in wave turbulence*, Phys. Rev. E **69**, 066608 (2004)
- [7] K. Hasselmann, J. Fluid Mech **12** 481 (1962).
- [8] V.E. Zakharov and Filonenko, J. Appl. Mech. Tech. Phys. **4** 506-515 (1967).
- [9] Y. Toba, J. Oceanogr. Soc. Jpn. 29, 209 (1973).
- [10] A.C. Newell, V.E. Zakharov, *Rough sea foam*, PRL **69** No.8, August 1992.
- [11] L. Biven, S.V. Nazarenko and A.C. Newell, "Breakdown of wave turbulence and the onset of intermittency" Phys Lett A, **280**, 28-32, (2001). A.C. Newell, S.V. Nazarenko and L. Biven, Physica D, **152-153**, 520-550, (2001).
- [12] Peter A.E.M. Janssen, *Nonlinear four-wave interactions and freak waves*, Journal of Phys.Oceanography, **33**, April 2003.
- [13] A.N. Pushkarev, On the Kolmogorov and frozen turbulence in numerical simulation of capillary waves, Eur. J. Mech. B/Fluids **18**, 345-352 (1999)
- [14] Choi, W. Nonlinear evolution equations for two-dimensional surface waves in a fluid of finite depth. J. Fluid Mech. 295, 381-394, (1995).
- [15] V.E. Zakharov, V.S. L'vov and G. Falkovich, "Kolmogorov Spectra of Turbulence", Springer-Verlag, 1992.
- [16] V.E. Zakharov, *Stability of periodic waves of finite amplitude on surface of deep water*, PMFT, No 2 (1968) 86-94.

- [17] V.E. Zakharov, *Inverse and direct cascade in the wind-driven surface wave turbulence and wave-breaking*, Proceedings of IUTAM Meeting on Wave Breaking (Sydney, 1991).
- [18] V.E. Zakharov, *Weakly nonlinear waves on the surface of an ideal fluid*, AMS Transl. **182**, 1998.
- [19] A.N. Pushkarev, D. Resio, V.E. Zakharov, *Weak turbulent approach to the wind-generated gravity sea waves*, Physica D 184 (1-4) 29-63 (2003).
- [20] V. P. Krasitskii, *On reduced equations in the Hamiltonian theory of weakly nonlinear surface-waves*, J. Fluid Mech. 272, (1994) 1.
- [21] B. Rumpf and L. Biven, *Weak turbulence and collapses in the Majda-McLaughlin-Tabak equation: Fluxes in wavenumber and in amplitude space*. Physica D 204 (2005), 188-203 (also on oai:arXiv.org:nlin/0503005).
- [22] E. Kartashova, *Wave resonances in systems with discrete spectra*, AMS Transl. (2) **182**, 1998.
- [23] O. M. Phillips, *On the dynamics of unsteady gravity waves of finite amplitude. 1. The elementary interactions* J. Fluid Mech. 9 (1960) 193.
- [24] Boris Pokorni, PhD thesis (2005).
- [25] C. Connaughton, S. Nazarenko, A. Pushkarev, *Discreteness and quasiresonances in weak turbulence of capillary waves*, Physical Review E, **63**, 046306, (2001).
- [26] S.N. Papakostas, Ch. Tsitouras, *High phase-lag-order Runge-Kutta and Nystrom pairs*, SIAM J.Sci.Comput. **21** No2, 1999.
- [27] V.E. Zakharov *Statistical theory of gravity and capillary waves on the surface of a finite-depth fluid*, Eur.J.Mech. B/Fluids, 1999.
- [28] A.I. Dyachenko, Y.V. Lvov *On the Hasselmann and Zakharov approaches to the kinetic equation for gravity waves*, J. Phy. Oceanography, **25**, No.12, December 1995.